Journal Pre-proofs



a Influence of heat treatment-induced residual stress on residual fatigue life of railway axles

P. Pokorný, P. Dlhý, J. Poduška, R. Fajkoš, T. Vojtek, L. Náhlík, M. Grasso, P. Hutař

PII: S0167-8442(20)30308-6
DOI: https://doi.org/10.1016/j.tafmec.2020.102732
Reference: TAFMEC 102732

To appear in: *Theoretical and Applied Fracture Mechanics*

Received Date: 3 March 2020
Revised Date: 3 July 2020
Accepted Date: 30 July 2020

Please cite this article as: P. Pokorný, P. Dlhý, J. Poduška, R. Fajkoš, T. Vojtek, L. Náhlík, M. Grasso, P. Hutař, a Influence of heat treatment-induced residual stress on residual fatigue life of railway axles, *Theoretical and Applied Fracture Mechanics* (2020), doi: https://doi.org/10.1016/j.tafmec.2020.102732

This is a PDF file of an article that has undergone enhancements after acceptance, such as the addition of a cover page and metadata, and formatting for readability, but it is not yet the definitive version of record. This version will undergo additional copyediting, typesetting and review before it is published in its final form, but we are providing this version to give early visibility of the article. Please note that, during the production process, errors may be discovered which could affect the content, and all legal disclaimers that apply to the journal pertain.

© 2020 Elsevier Ltd. All rights reserved.

Theoretical and Applied Fracture Mechanics, Volume 109, October 2020, Article number 102732
DOI:10.1016/j.tafmec.2020.102732

Influence of heat treatment-induced residual stress on residual fatigue life of railway axles

P. Pokorný[a*], P. Dlhý[a,b], J. Poduška[a], R. Fajkoš[c], T. Vojtek[a,b], L. Náhlík[a], M. Grasso[d,e], P. Hutař[a]

[a] Institute of Physics of Materials, Academy of Sciences of the Czech Republic, v. v. i., Žižkova 22, 616 62 Brno, Czech Republic

[b] Central European Institute of Technology (CEITEC), Brno University of Technology, Purkyňova 123, 612 00 Brno, Czech Republic

[b] BONATRANS GROUP, a. s., Revoluční 1234, 735 94 Bohumín, Czech Republic

[d] University of Hertfordshire, Hatfield, Hertfordshire, AL10 9AB, United Kingdom

[e] School of Aerospace, Transport and Manufacturing, Cranfield University, MK43 0AL, United Kingdom

*email: pokorny@ipm.cz

Abstract

Assessment of residual fatigue life of railway axles commonly does not include effect of residual stress. This paper presents advanced methodology for estimation of residual fatigue life of railway axles considering not only external loading but also internal residual stresses. The studied axles made of the EA4T steel were treated by induction hardening in order to generate very high compressive residual stress in the surface layer of the axle. Such residual stress has positive effect on behaviour of surface defects and leads to fatigue crack retardation or even crack arrest and, consequently, to immense prolongation of residual fatigue life. Experimentally measured data of residual stress were implemented in a numerical model in order to determine the true stress state in the axle. The model included a crack and took the effects of bending, press fit and residual stress into account. Residual fatigue life was calculated for various starting crack lengths based on the experimentally determined da/dN-ΔK curves for various load ratios. Finally, the results for axles hardened by standard method and by induction hardening were compared with residual fatigue lives obtained experimentally from fatigue tests on real railway axles with artificial cracks. The calculated values were conservative with good agreement with experimental data.

Keywords: Railway axle, fatigue life prediction, residual stress, fatigue crack propagation, hardening

Published by Elsevier. This is the Author Accepted Manuscript issued with: Creative Commons Attribution Non-Commercial No Derivatives License (CC:BY:NC:ND 4.0).
The final published version (version of record) is available online at DOI:10.1016/j.tafmec.2020.102732. Please refer to any applicable publisher terms of use.

Nomenclature:

a	length of crack
a_0	length of initial crack
a_f	length of final crack
a_n	length of considered notch
a_i	crack length in i-th loop
a_{i-1}	crack length in (i-1)th loop
b	parameter describing crack front shape
b_0	½ width of initial crack
b_f	½ width of final crack
b_n	½ width of considered notch
C	fitting parameter of the NASGRO equation
da/dN	fatigue crack propagation rate
E	Young's modulus
F	applied force
k	dynamic coefficient
K_a	amplitude of stress intensity factor in load cycle
$K_{B,d}$	stress intensity factor corresponding to dynamic bending load
$K_{B,s}$	stress intensity factor corresponding to static bending load
K_I	value of mode I stress intensity factor
K_m	mean value of stress intensity factor in load cycle
K_{max}	maximal value of stress intensity factor in load cycle
$K_{max,th}$	threshold value in K_{max} expression
K_{min}	minimal value of stress intensity factor in load cycle
K_{PF}	stress intensity factor corresponding to press-fit load
K_{RS}	stress intensity factor corresponding to residual stress load
n	fitting parameter of the NASGRO equation
p	fitting parameter of the NASGRO equation
R	load ratio
S_i	stress determined by drilling method
t	time/specimen thickness
u_x, u_y, u_z	displacements in x ,y and z directions
W	half of CCT specimen width
x, y, z	Cartesian coordinates
Δa	crack length increment
ΔK	stress intensity factor range
ΔN	increment of load cycles
μ	contact friction coefficient
v	Poisson's ratio

Abbreviations:

FE	finite element
PF	press fit
RFL	residual fatigue life
RS	residual stress
SIF	stress intensity factor

1 Introduction

Railway axles are cyclically loaded components exposed to various mechanical loads and environmental conditions during long-term service. According to [1] it is not exceptional that railway axles stay in service for 30 years or even more. During such a long period fatigue failure of railway axles can occur, see e.g. [2] or [3]. Fatigue cracks are often initiated in corrosion pits or damage areas (both cases causing crack initiation at axle surface) caused by ballast impacts during operation of railway axle, see [1]. The number of train accidents in the European Union due to axle failures was 34, 18 and 14 in the years 2012, 2013 and 2014 respectively according to the European Union Agency for Railways Report (2016) [4]. The main aim of train manufacturers and operators is to reduce the number of such accidents. For safe operation of trains it is necessary to consider presence of such defects in the axles, see e.g. [5–7] . Therefore, damage tolerance approach considering presence of cracks is often applied to estimate the number of loading cycles needed for fatigue crack propagation from its initial size up to the critical one. The considered initial crack length corresponds to the probability of detection of the used non-destructive inspection method. These methods still cannot detect the defects with 100% probability. Regular inspection intervals including non-destructive testing for revealing of potential defects are set up based on the estimated residual fatigue life (RFL). Frequent inspections (short inspection intervals) would reduce the risk of a fatigue failure. However, too frequent inspections lead to additional maintenance costs. Therefore, a more precise estimation of RFL of railway axles would be beneficial for both safe operation and maintenance costs. These challenging requirements are discussed in various recently published papers related to crack growth in railway axles and used materials, e.g. [8–16].

The residual stress can significantly influence fatigue resistance of engineering components. Positive or negative impact of residual stress is dependent on the sign and direction of the residual stress relative to the applied stress, i.e. on whether it adds to, or subtracts from, the applied stress [17]. In the case of railway axles a certain amount of residual stress is always induced by machining or heat treatment. However, the residual stress magnitudes vary from relatively small values up to hundreds of MPa which also changes significantly stress distribution in the whole cross section of the axle. Compressive axial residual stress in the axle surface area is way to increase resistance to initiation of surface defects and to slow down or completely stop propagation of fatigue cracks, see e.g. [18–20]. It was found that RFL of railway axles is dominantly given by propagation of relatively short cracks (up to 5 mm) near the surface, see e.g. [21]. Therefore, significant effect of subsurface compressive residual stress on fatigue crack initiation and propagation of surface cracks is expected.

Almost all researchers calculating RFL take into account loading of the axle by bending (train weight + dynamic effects of moving train), some of them consider even the press fit load [22–25]. However, in most of the cases they do not consider residual stress, which is important. In the presented work it was managed to take residual stress into account due to advanced experimental and numerical techniques. The theoretical basis for current research was laid in [26], where the procedure how take into account the effects of residual stress on the residual fatigue life of railway axles was presented. However, the residual stress field was based only on theoretical considerations. In the present paper, a special method of combination of experimental measurement on particular heat-treated axle pieces and numerical modelling was carried out in order to determine residual stress. Afterwards, the results were compared to RFLs obtained from experiments on real axles.

Subsurface residual stress can be induced in the axle, e.g. by deep rolling, shot peening, machining, heat treatment etc. These procedures lead to different distributions and magnitudes of residual stress, see Table 1. For example, in the case of the railway axle steel EA4T, deep rolling provides residual stress field with the maximum compressive stress ca. 640 MPa, see [18] or [19]. However, this treatment leads to a very high gradient of residual stress close to the surface. In the depth of 3 mm the residual stress changes from compressive to tensile stress. Therefore, in quite small depth under the axle surface the positive influence of deep rolling disappears. According to [20] it is possible to develop residual stress field with maximum compressive stress value of about 60 MPa in the case of standardly manufactured railway axle with consequent heat treatment and machining. The compressive residual stress extends to the depth of 22 mm under the surface where it turns into tensile stress. It means that residual stress after manufacturing, heat treatment and final machining is not as high as in the case of deep rolling but they affect a larger volume of material below the axle surface. Authors in [27] deals with effect of shoot peening and grinding on residual stress in EA4T and EA1N steels.

Besides EA4T steel data, residual stress distributions for other railway axle materials can be found in literature. Zhang et al. [28] reported distribution of residual stress in bars from Chinese standard steels 35CrMoSP and 50SP after shot peening. In these cases, the highest absolute values of compressive stress are 750 MPa and 560 MPa respectively. Nevertheless, according to [28] the compressive stress extends to the depth of only 0.1 mm below the surface (note that these experiments were performed on small specimens with the shot peened diameter of 4 mm). Makino et al. [29] and Isomura et al. [30] showed distributions of residual stress in induction-hardened railway axles made of JIS S38C steel. In this case the maximum compressive stress values ranged from 200 MPa to 600 MPa and the depth of compressive layer ranged from 4 to 18 mm depending on parameters of induction hardening technique. Residual life assessment of induction hardened railway axles (with residual stresses obtained by modelling) from material 34CrNiMo6 was carried out in [31] and 35CrMo in [32]. Table 1 compares different methods of surface treatment. One can see that the induction-hardening generates very high compressive residual stress and the affected area is significantly deeper than in the case of shot peening or deep rolling. Therefore, this work is focused on induction hardening as a technology improving the fatigue strength of railway axles.

Table 1 – Parameters of compressive residual stress for different technologies of surface treatment

paper	material	method of surface treatment	diameter of tested specimen	maximal compressive axial stress	depth with zero RS
[18] Regazzi et al. (2014)	EA4T	deep rolling	130 mm	≈ 640 MPa	≈ 3 mm
[19]- Hassani-Gangaraj et al. (2015)	EA4T	deep rolling	172 mm	≈ 640 MPa	≈ 3 mm
[20]- Gänser et al. (2016)	EA4T	conventional manufacturing, heat treatment and machining	190 mm	≈ 60 MPa	≈ 22 mm
[27] – Lorang et al. (2018)	EA4T	shot peening	bar specimen	≈ 400 MPa	≈ 0.2 mm
[27] – Lorang et al. (2018)	EA4T	grinding	bar specimen	≈ 100 MPa	≈ 0.075 mm
[27] – Lorang et al. (2018)	EA1N	shot peening	bar specimen	≈ 400 MPa	> 0.25 mm
[27] – Lorang et al. (2018)	EA1N	grinding	bar specimen	≈ 30 MPa	≈ 0.05 mm
[28]- Zhang et al. (2011)	50SP	shot peening	4 mm	≈ 750 MPa	≈ 0.1 mm
[28]- Zhang et al. (2011)	35CrMo	shot peening	4 mm	≈ 560 MPa	≈ 0.1 mm
[29]- Makino and Sakai (2013) or [30]- Isomura and Yomoda (1995)	JIS S38C	induction hardening	166 mm	≈ 200–600 MPa	≈ 4–18 mm
[32] Gong et. al	35CrMo	induction hardening	120 mm	≈ 200 MPa	≈ 8 mm
[31] Wu et al.	34CrNiMo6	induction hardening	120 mm	≈ 200 MPa	≈ 8 mm

2 Determination of residual stress

Design of the investigated railway axle made of the EA4T steel is depicted in Fig. 1. Two axles manufactured using conventional heat treatment with consequent machining and two axles treated by induction hardening were investigated. The distribution of residual stress in the surface layer was measured by means of the drilling method using the drilling head VISHAY RS-200 (Fig. 2), the 3-grid strain gauge rosettes HBM RY21-3/120 and the HBM SPIDER8-30 measurement system. Drilling method is typical technique for determination of residual stress see e.g. [33].

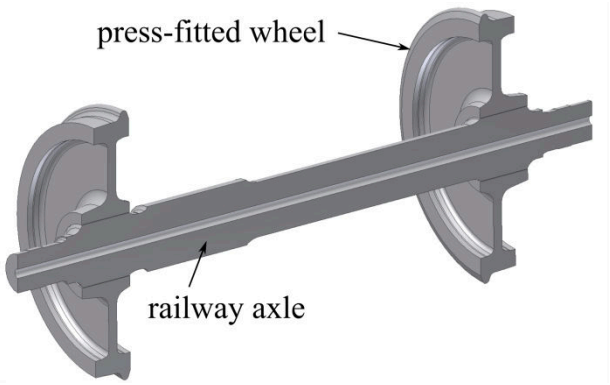


Fig. 1 – Investigated railway axle manufactured from steel EA4T

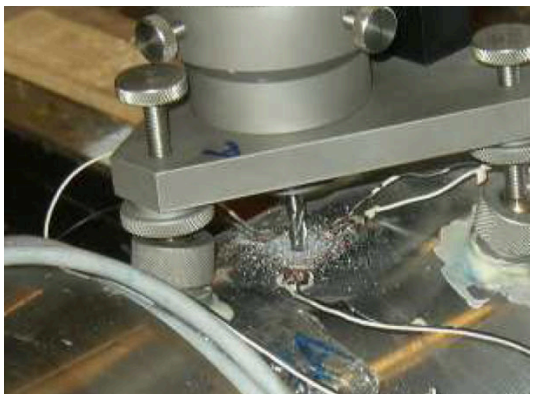


Fig. 2 – Drilling head VISHAY RS-200 and detailed view of the axle drilling

2.1 Residual stress in conventionally heat-treated railway axles

The residual stress field was measured in three points at the axle surface (see Fig. 3) in the case of conventionally heat-treated axles with subsequent machining. The residual stress was measured up to the depth of approx. 2.5 mm below the axle surface at each point. Two axles from two different batches were used for residual stress measurement.

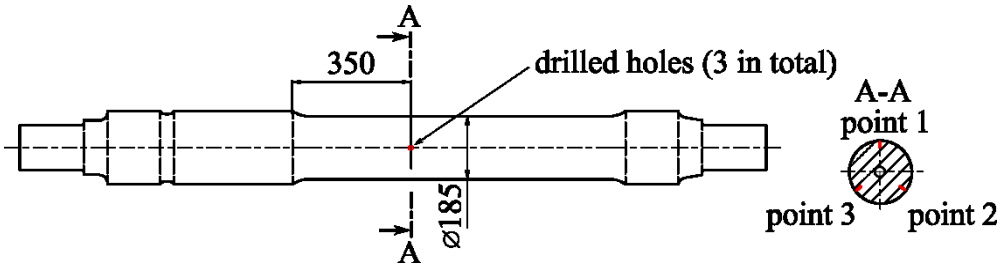


Fig. 3 – Position of the drilled holes at the axle and a detailed view of three holes in the cross section

Axial (longitudinal) stress and hoop (tangential) stress were determined using the 3-grid strain gauge rosettes and the results are presented in Fig. 4. Axial stress and hoop stress exhibited similar distributions in the surface layer. Both were negative within the investigated area (depth

from 0 to 2.5 mm) and the maximum absolute values were in the depth of ≈1 mm below the surface. These peak values were in the range from –45 to –65 MPa for axial stress and from –55 to –70 MPa for hoop stress.

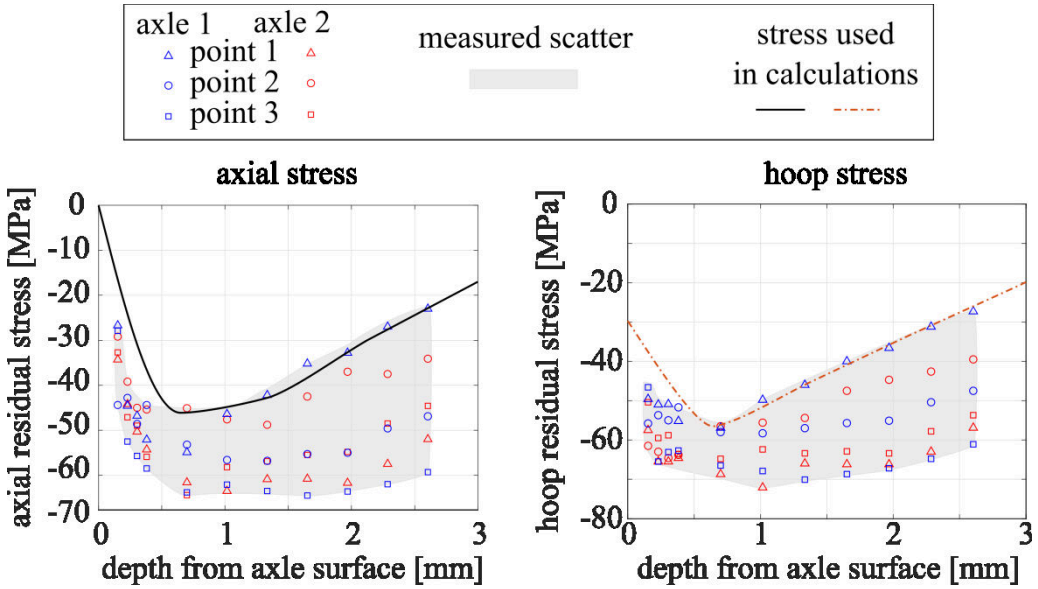


Fig. 4 – Measured residual stresses in the surface layer of conventionally heat-treated axles

The scatter of residual stress distributions visible in Fig. 4 is given by differences between the two axles as well as differences between data from three measurement positions along the circumference. For conservative estimation of residual fatigue life, the lowest absolute values of residual stresses were used.

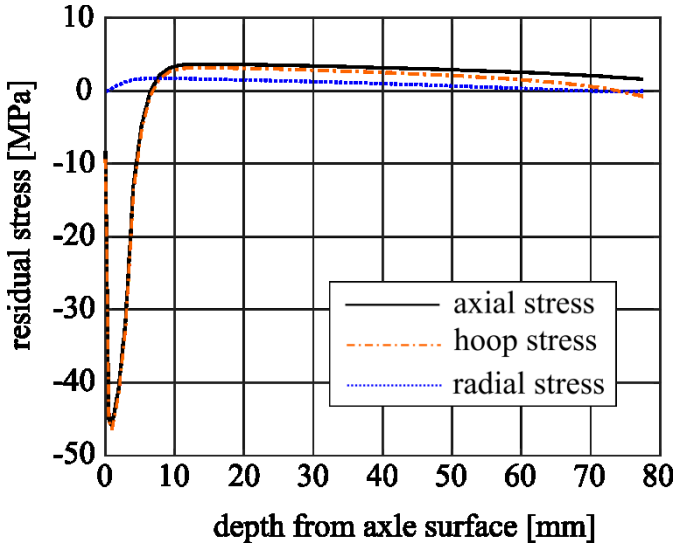


Fig. 5 – Determined profiles of residual stresses in conventionally heat-treated axles

The maximum depth of the measurements (2.5 mm) was given by limitations of drilling method used, see reference [34]. The measured data were extrapolated for depths larger than 2.5 mm and corrected by numerical calculations to obtain realistic residual stress profiles in the whole cross section. Final stress distribution profiles (see Fig. 5) were reached by finite element (FE)

iterative modelling which respected the measured stress values at the axle surface and the equilibrium of forces and moments in the whole cross section of the axle. Final profiles used in the following estimation of residual fatigue life were conservative (see Fig. 4 for comparison).

2.2 Residual stress in induction-hardened railway axles

In the case of induction-hardened axles, the magnitude and penetration of residual compressive stress are much higher compared to the conventionally heat-treated axles. Due to this, the standard drilling measurement from external surface was not sufficient (limitation to the depth of 2.5 mm). For this reason, the axle body was divided into 5 sections. Each section was gradually turned from the original diameter (185 mm) removing a 5 mm layer (10 mm in diameter), as shown in Fig. 6. The purpose of that was to determine residual stress in these particular depths below the axle surface. This was done again by the drilling method making holes in the middle of each turned section, see Fig. 6.

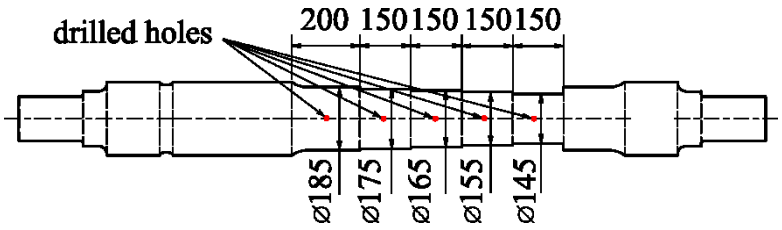


Fig. 6 – Positions of the drilled holes at gradually turned sections of the induction-hardened axle

The stresses measured by the 3-grid strain gauge rosettes are shown in Table 2. They were negative in whole range of measured depths i.e 0-20 mm below the axle surface and the highest absolute values were in the depth of 5 mm with the hoop stress of –989 MPa and the axial stress of –951 MPa.

Table 2 – raw residual stress (without post-processing) measured at sections of gradually turned induction hardened axle

position of 3-grid strain gauge	axial stress [MPa]	hoop stress [MPa]
diameter 185 mm (axle surface)	–634	–729
diameter 175 mm (depth 5 mm)	–951	–989
diameter 165 mm (depth 10 mm)	–304	–367
diameter 155 mm (depth 15 mm)	–239	–280
diameter 145 mm (depth 20 mm)	–207	–230

Since the turning does not remove only material but also partially the residual stresses, the data shown in Table 2 have to be post-processed by FE modelling in order to determine residual stress distributions in original state of the railway axle.

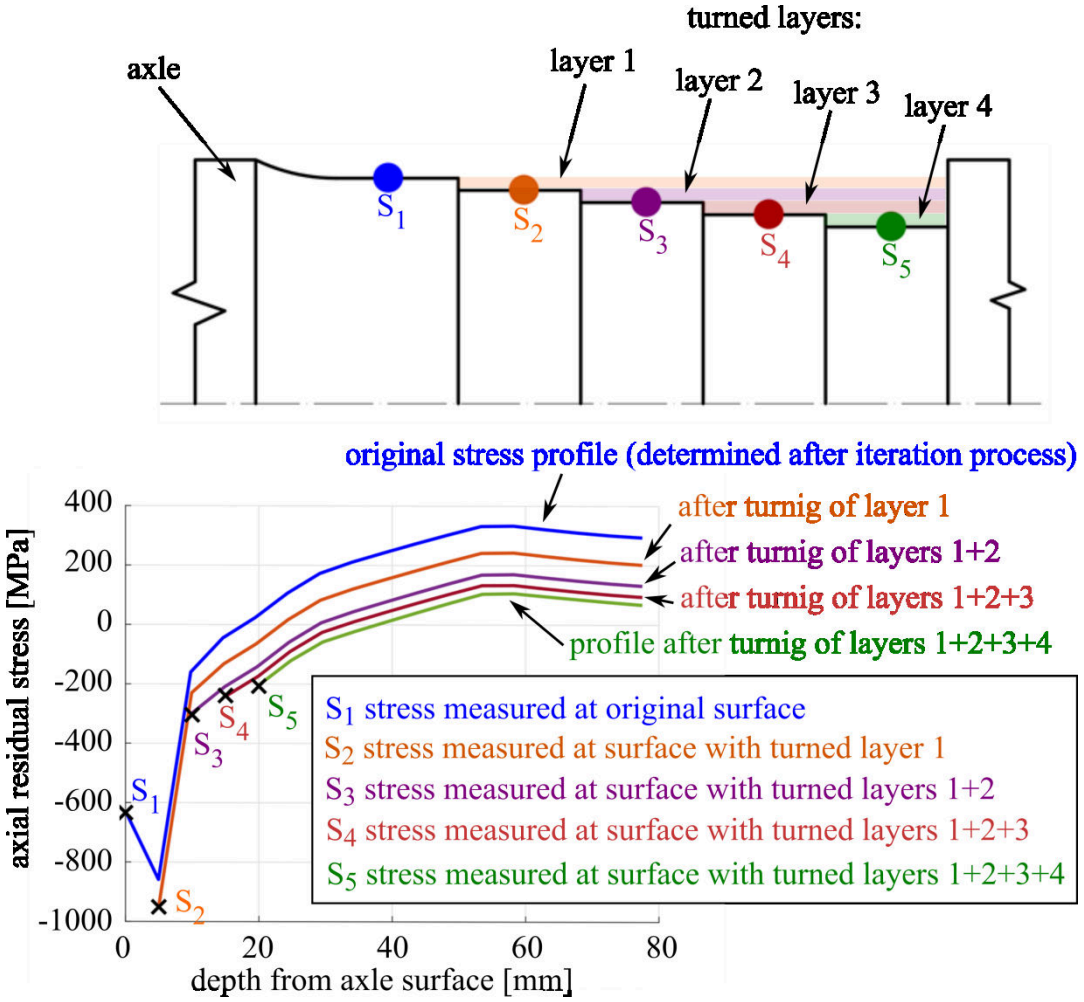


Fig. 7 – Scheme of the post-processing of measured data to obtain residual stress profiles after induction hardening (example for axial stress)

A FE model of the measured axle (with turned layers according to Fig. 6) was created to determine the residual stress profile in the original railway axle (without turned sections). Since axial symmetry of the residual stress distribution can be considered, a 2D axisymmetric FE model was used. Based on the measured data (see Table 2) as well as literature [30], it was expected that the largest gradients of residual stresses would be close to the axle surface. Therefore, FE mesh was inhomogeneously distributed along the cross section with the finest mesh in the axle surface area. The smallest element size was 0.2 mm and the FE model contained circa 400 000 nodes in total. It was assumed that the residual stress distributions in vicinity of the axle surface were constant along the longitudinal direction. The model included elastic material properties corresponding to the EA4T steel; the Young's modulus $E = 205$ GPa and the Poisson's ratio $\nu = 0.3$.

The iteration process followed, where the expected values of residual stresses (axial, hoop and radial) were defined in the nodes as functions of the distance from the original axle surface (without turned sections). The prescribed values were first estimated based on the measured values (Table 2) and then computed by the iteration process as follows. The computed residual stress profile (blue curve in Fig. 7) had to comply these conditions:

1) The searched original residual stress profile (residual stress in the non-turned axle) has to start at the same value S_1 that was measured at the axle surface, see Fig. 7 and Table 2.
2) Balance between positive and negative residual stresses (forces and moments) has to be satisfied.
3) If the found stress profile is correct (see blue curve in Fig. 7) and some layers are removed in the FE model (see Fig. 7) the stresses at such turned axle surface have to correspond to the measured ones (e.g. the orange curve in Fig. 7 shows redistributed stress profile after turning of layer 1).

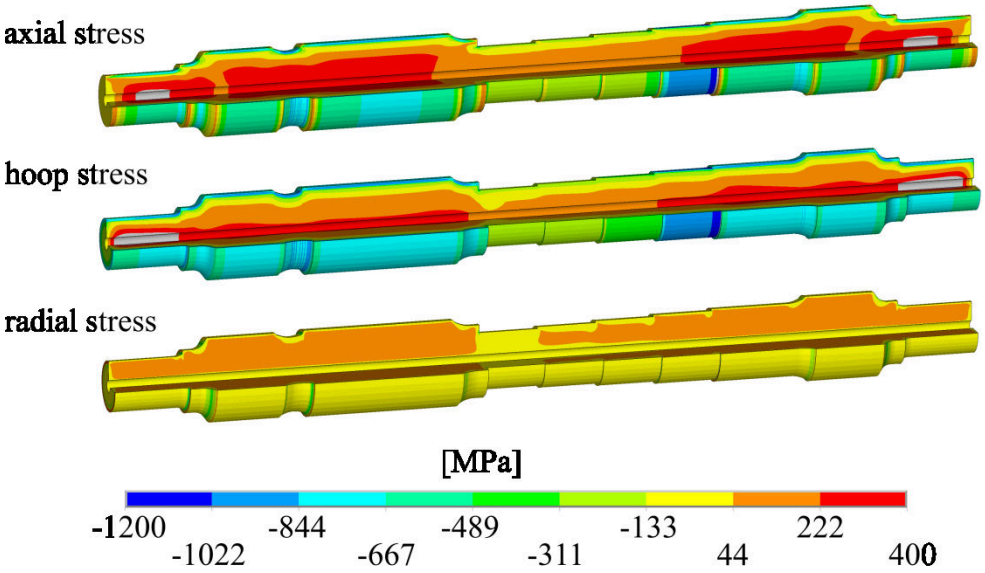


Fig. 8 – Results of residual stresses in turned axle section after iteration process

The procedure described in the previous paragraph was done for both axial and tangential stress. Both profiles were found by iteration process in the FE model so that the stress profiles complied the measured data. Note that radial stress was zero at each surface of the turned layers. However, in the non-turned axle the radial stress was non-zero below the axle surface. The radial distribution of the residual stress resulted from the static equilibrium of forces and moments. Fig. 8 shows the used FE model with turned sections after the iteration process for all mentioned components of stress (axial, hoop and radial). Fig. 9 shows determined residual stress distributions in the original axle (without turned sections). It is worth to point out that the true residual stress profile (blue curve in Fig. 7 with the peak of -850 MPa) exhibited smaller magnitudes of compression axial stress than the measured values below original axle surface (S_2, S_3, S_4 and S_5) with the peak of -950 MPa, see Table 2. Therefore, the measured data cannot be directly used for residual fatigue life estimation. Redistribution of stress has to be considered, otherwise the results would be non-conservative.

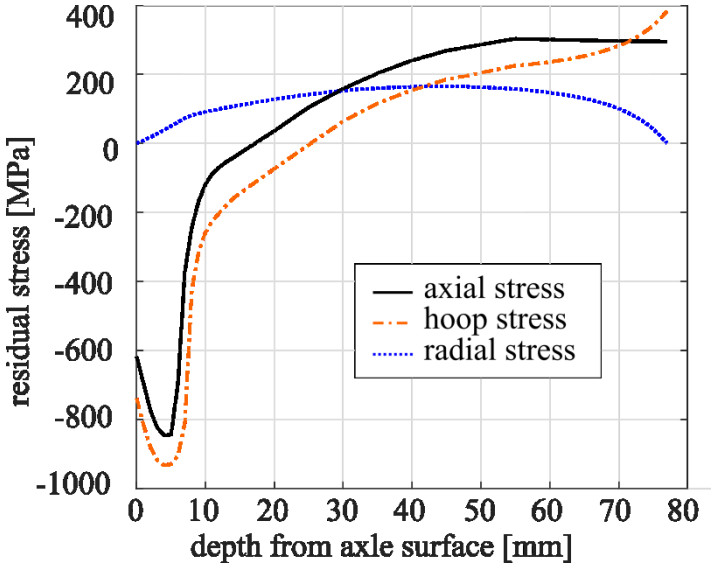


Fig. 9 – Determined profiles of residual stresses in induction hardened railway axles

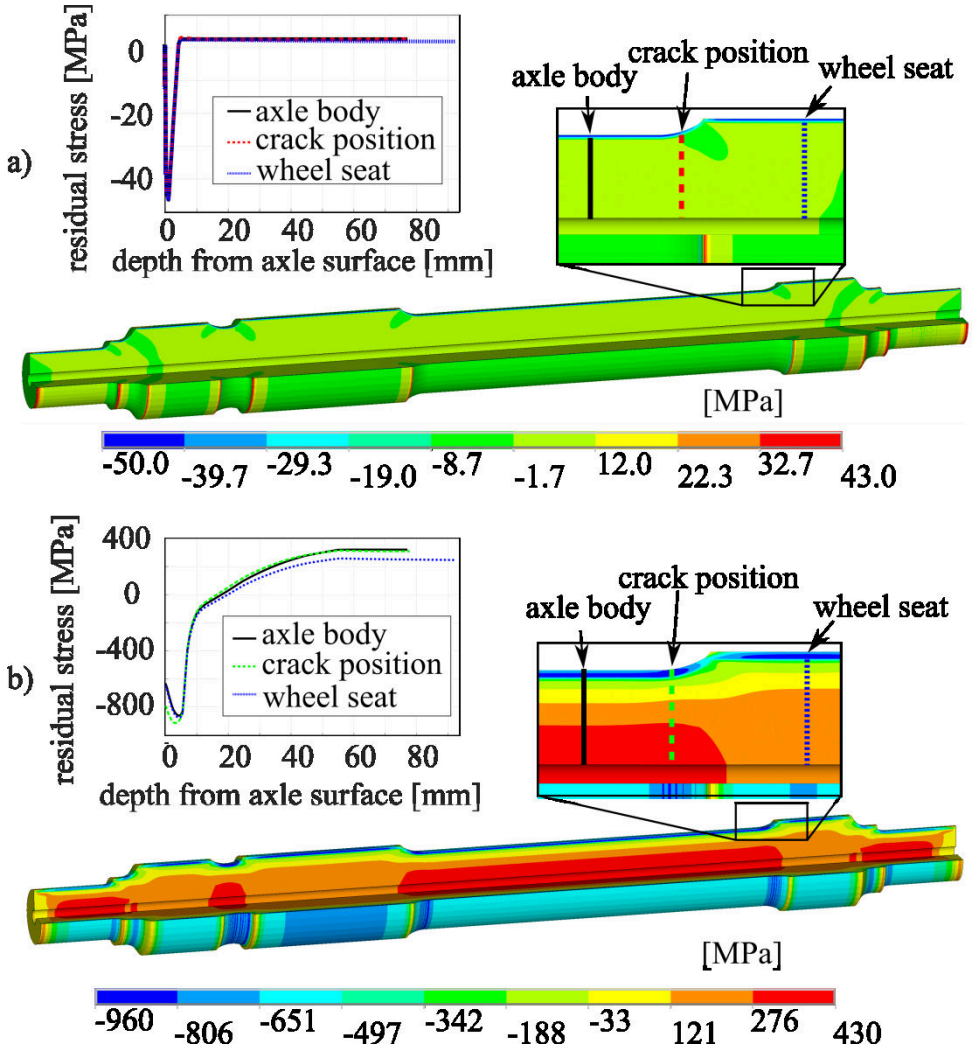


Fig. 10– residual axial stress in a) standard heat treated axle b) induction hardened axle

The presented results were obtained for the axle body with non-varying diameter, where residual stress is possible to measure. However, in the RFL estimation, a crack was considered in the radius transition between the axle body and the wheel seat. Therefore, due to geometry transitions, stress concentration (T-notch) and static equilibrium, there is a slightly different redistribution of residual stresses compared to axle body. Since the FE model was done for the whole axle, it already included also the redistributed stress field in all cross sections of axle. Fig. 10 shows redistributed residual stress profiles in the axial direction for both considered types of heat treatment: conventional heat treatment and induction hardening. This figure also depicts different profiles for the axle body, wheel seat and the T-notch. Table 3 summarizes the obtained maximum values of axial stress, which is the most important component for fatigue performance.

Table 3 – Magnitudes of compressive axial stress for given heat treatment

heat treatment	experimentally determined peaks	depth with zero residual stress
standard hardening	≈ –45 to –65 MPa	≈ 7 mm
induction hardening	≈ –850 MPa	≈ 18 mm

3 Estimation of residual fatigue life of railway axles considering residual stress

A key aspect for a reliable estimation of residual fatigue life of railway axles is the identification of the location where a potential crack would cause the shortest RFL. There are three important loading components of the railway axle:

- bending load (caused by weight and movement of the vehicle)
- press-fit load (caused by press-fitted joint between axle and wheels)
- residual stress load (caused dominantly by heat treatment and machining)

The residual stress is more or less uniformly distributed along the longitudinal direction of the axle and is supposed to be constant during the lifespan of the axle. The press-fit load is given by the press-fit joint between the axle and the wheel. These two loading components affect the mean stress of the total loading. From the point of view of fatigue, the most important component of loading is the cyclic bending produced by the vehicle weight and the superimposed dynamic effects caused by its movement. Bending loading due to the weight can be estimated by means of FE analysis and it corresponds to the train running slowly on a straight track where dynamic forces can be neglected. Dynamic bending load is taken into account by considering of load spectrum which was experimentally measured for typical trains and rail tracks.

Based on the loading situation, it can be expected that the critical position for cracking corresponding to the shortest fatigue life would occur in one of the notches close to the press-fitted wheel due to superposition of bending load with press-fit load and stress concentration in the notch. The above assumption was verified by means of FE analysis. A simplified model without a crack was implemented to identify the critical positions for the crack initiation and fast propagation (Fig. 11). This model takes into account the weight of the vehicle and the press-

fitted wheel. The interference value between the press-fitted wheels and the axle was assumed to be 0.3 mm in diameter. A non-linear contact with the friction coefficient μ = 0.6 was considered in the FE model. Details of the contact modelling can be found in [21] or [22]. The FE model consisted of approximately 790 000 nodes and 178 000 elements.

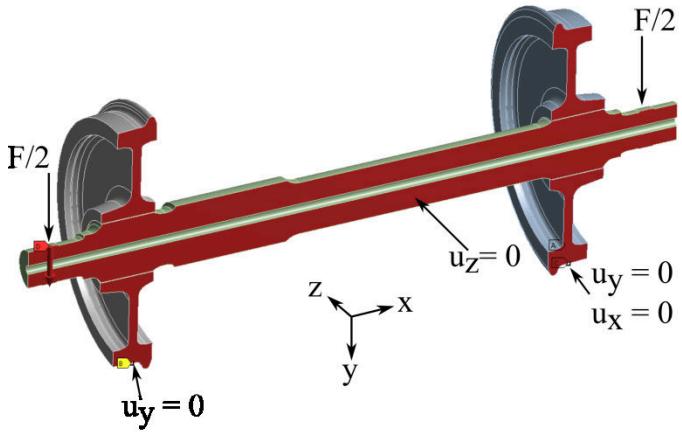


Fig. 11 – Boundary conditions for determination of critical position of fatigue crack

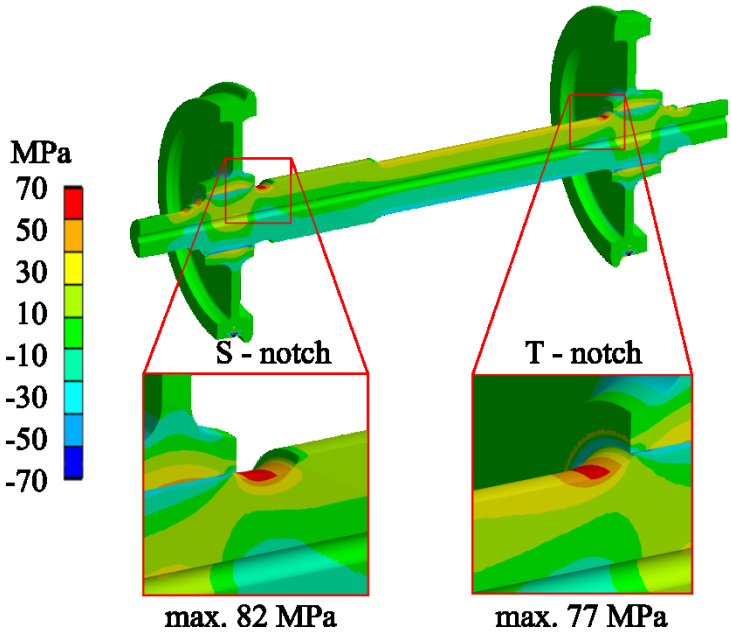


Fig. 12 – Results of weight load and press-fit load (axial stress)

The force F = 82 300 N was applied to each of the two axle journals (corresponding to weight load of 16.5 ton per axle). The boundary conditions are shown in Fig. 11. It was possible to model only one half of the railway axle due to symmetry of geometry and loading. In the reduced model, the force $F/2$ was applied to the axle journals. Results of the FE analysis for bending loading and press-fit loading are presented in Fig. 12. As expected, the critical positions for potential crack were at so called the S-notch and the T-notch. The highest axial stress value at the S-notch was approximately 82 MPa and at the T-notch it was 77 MPa. It is not possible to assume that a fatigue crack at the S-notch would be certainly more detrimental than that at the T-notch. Fatigue crack growth is not only influenced by the maximum stress value at the surface but also by stress distribution below the axle surface. Therefore, both notches are

dangerous for initiation and growth of fatigue cracks. In this paper, the presence of a crack only at the T-notch is assumed in order to compare the results with the experiments on axles with artificial cracks generated at the T-notch.

After determination of the critical position, three sets of numerical models of the axle including a fatigue crack were implemented for pure bending, press-fit and residual stress loading. The driving force parameter for crack growth under Linear Elastic Fracture Mechanics (LEFM) was the stress intensity factor K (SIF), see e.g. [35]. The assumption of LEFM allowed the use of the superposition principle. The mutual separation of the three external loads led to the expression (1) of the total SIF K_{max} in the form:

$$K_{max}(a,t) = K_{B,d}(a,t) + K_{PF}(a) + K_{RS}(a), \quad (1)$$

where $K_{B,d}$ is the SIF due to dynamic bending load (depending on crack length a and load spectrum), K_{PF} is the SIF due to press-fit load and K_{RS} is the SIF corresponding to residual stress load.

3.1 Loading of a crack at the T-notch caused by dynamic bending of the axle

The stress intensity factor corresponding to the bending load was calculated using FE model. This model had the same symmetry and boundary conditions as those shown in Fig. 11. Such model considered only the bending load with no press-fit of the wheels. The crack front was approximated by a semi-ellipse with changing aspect ratio according to [21] and the orientation of the crack was perpendicular to the longitudinal axis of the axle (perpendicular to the highest principal stress).

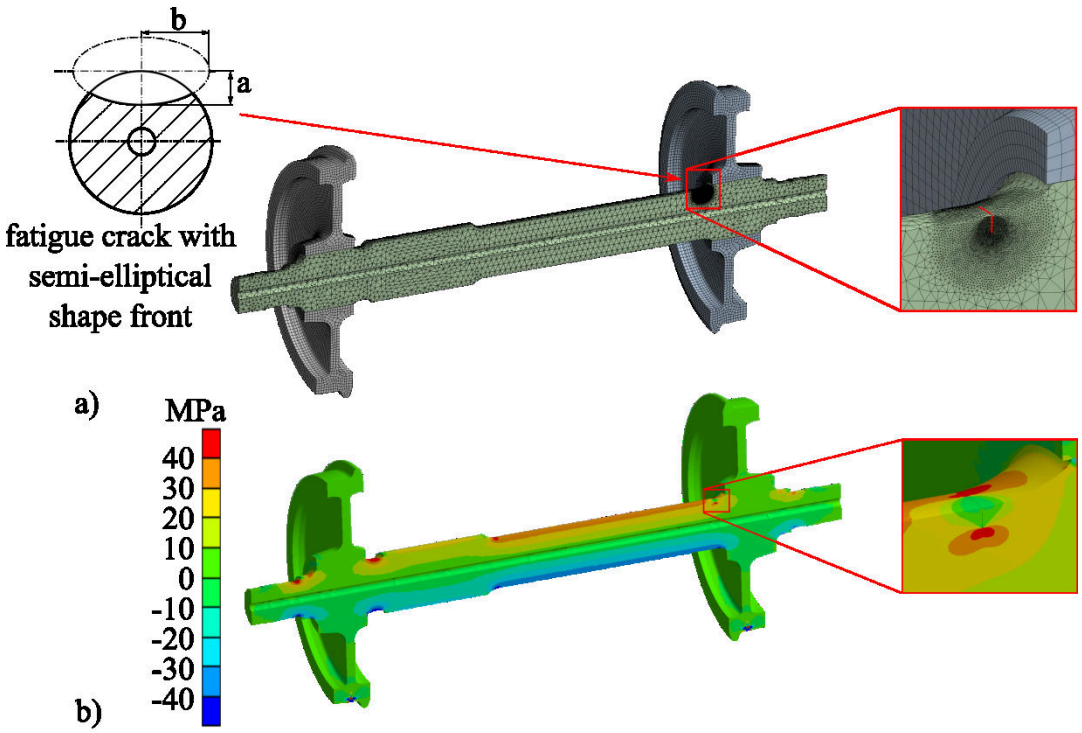


Fig. 13 – Mesh of model and result of bending load (axial stress) for axle with semi-elliptical crack at the T- notch

A crack was modelled at the T-notch with 23 different lengths from a = 2 mm to 25 mm (see parameter a in Fig. 13a). It was assumed that propagation up to the crack length of 25 mm covers more than 95% of the total residual fatigue life [21]. Fig. 13a shows the discretization used in the FE model and Fig. 13b shows the result of the axial stress component for the crack length a = 10 mm. The mesh of 20 nodes solid elements (SOLID 186) was substantially refined around the crack to obtain more accurate results of the SIFs. On the basis of the axial stress distribution, the SIF values corresponding to the bending load $K_{B,s}$ (static case), were determined according to the procedure described in [21].

Variable-amplitude loading caused by the train movement is described by a load spectrum. The load spectrum used for the numerical analysis in this work is shown in Fig. 14 [13]. The so called dynamic coefficient k corresponding to multiple of the static load $K_{B,s}$ (load due to the nominal vehicle weight) is on the vertical axis. The horizontal axis refers to a cumulative number of cycles, i.e. the number of cycles with a higher dynamic coefficient than that at the particular point of the spectrum curve.

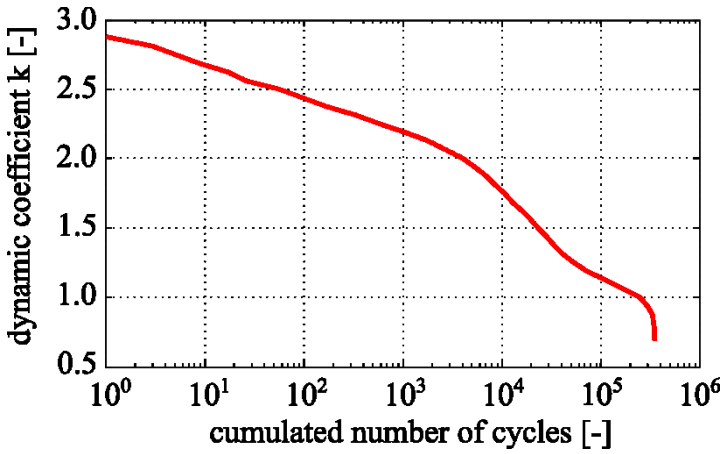


Fig. 14 – Load spectrum describing the bending load in terms of the dynamic coefficient k. The number of cycles refers to 1000 km of train operation [13]

The dynamic bending load $K_{B,d}$ is given by:

$$K_{B,d}(a,t) = k(t).K_{B,s}(a), \tag{2}$$

where k is the dynamic coefficient and $K_{B,s}$ is the SIF corresponding to the static bending load.

Results of $K_{B,d}$ as a dependence on the crack length a (for the highest dynamic coefficient k = 2.9) are presented in Figs. 17 and 18.

3.2 Loading of a crack at the T-notch caused by the press fit

The press-fit load K_{PF} was modelled considering a contact interference between the axle and the wheel (non-linear contact FE model). The methodology was adopted according to [21]. The interference between the press-fitted wheels and the axle was set to 0.3 mm and the contact

friction coefficient was set to $\mu = 0.6$ (the same values as were used for critical crack position determination). The FE mesh and 23 different crack lengths (from $a = 2$ mm to 25 mm) created in the model in the same way as in the case of the bending load (Fig. 13a). Contours of the result of the axial stress solution are presented in Fig. 15. Results of K_{PF} as a dependence on the crack length a were plotted in Figs. 17 and 18.

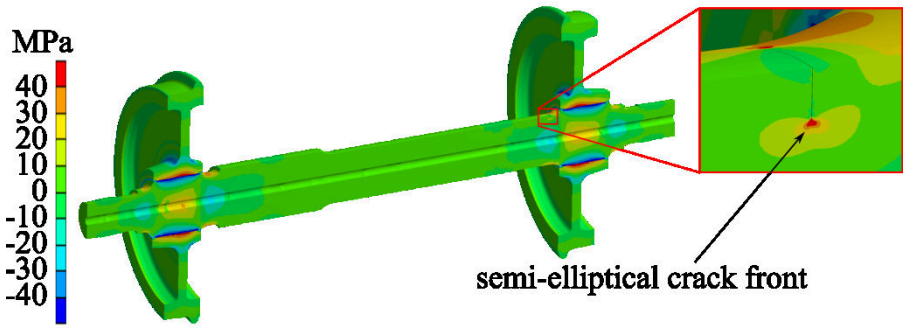


Fig. 15– Result of the longitudinal stress caused by the press-fit for axle containing a semi-elliptical crack at the T-notch

3.3 Loading of a crack at the T-notch caused by the residual stress

It was considered, that residual stress profiles determined in Section 2 were homogeneous along the axial direction of the axle and axisymmetric. Due to the fact that the diameters of the axle body and the wheel seats are not identical, the residual stress profiles in these areas are slightly different, see Fig. 10. Since the residual stress distribution exhibits rapid gradients, it was necessary to use a model with a finer mesh than in the models for considering bending and press-fit loads. In order to obtain results of SIFs caused by residual stress load in reasonable time, a partial FE model of the axle (including crack) was created, as shown in Fig. 16. This model included stress fields obtained in the previous model, see Fig. 10.

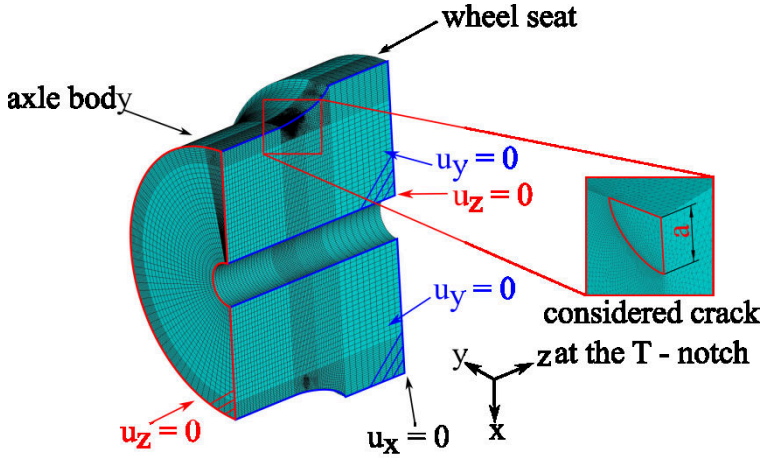


Fig. 16 – Partial model of the considered railway axle used for determination of stress intensity factor caused by the presence of residual stress

By creating of a semi-elliptical crack at the T-notch, the stress was redistributed around the crack area and the SIF corresponding to the residual stress field K_{RS} was determined by the

FE model. This model also included only one half of the axle part due to symmetry. The refined mesh of 20 nodes solid elements (SOLID 186) around the crack and the boundary conditions are shown in Fig. 16. Equal number of crack lengths 23 as in the previous cases were modelled (from 2 mm to 25 mm) for both types of heat treatments described in Section 2 (46 models in total). The resulting SIFs were negative and they are plotted as a dependence on the crack length a in Figs. 17 and 18. Note that conservative stress distribution (upper envelope in Fig. 4) was used for determination of K_{RS} in the standard hardened axle in Fig. 17. These negative values superimposed to the positive values resulting from bending and press-fit loads generate total loading.

3.4 Total load of the railway axle

The total SIF values were calculated by means of the superposition principle of all components (bending, press-fit and residual stress load):

$$K_{max}(a,t) = K_{B,d}(a,t) + K_{PF}(a) + K_{RS}(a).$$

Each component of SIF is a function of the crack length a. The sum of press-fit and residual stress loads represents the mean SIF K_m:

$$K_m(a) = K_{PF}(a) + K_{RS}(a). \quad (3)$$

The amplitude of the total SIF is represented by the dynamic bending load $K_{B,d}$:

$$K_a(a,t) = K_{B,d}(a,t) = k(t).K_{B,s}(a). \quad (4)$$

The minimum and maximum SIFs during the load cycle are given by the following equations:

$$K_{min}(a,t) = K_m(a) - K_a(a,t) = K_{PF}(a) + K_{RS}(a) - K_{B,d}(a,t), \quad (5a)$$

$$K_{max}(a,t) = K_m(a) + K_a(a,t) = K_{PF}(a) + K_{RS}(a) + K_{B,d}(a,t). \quad (5b)$$

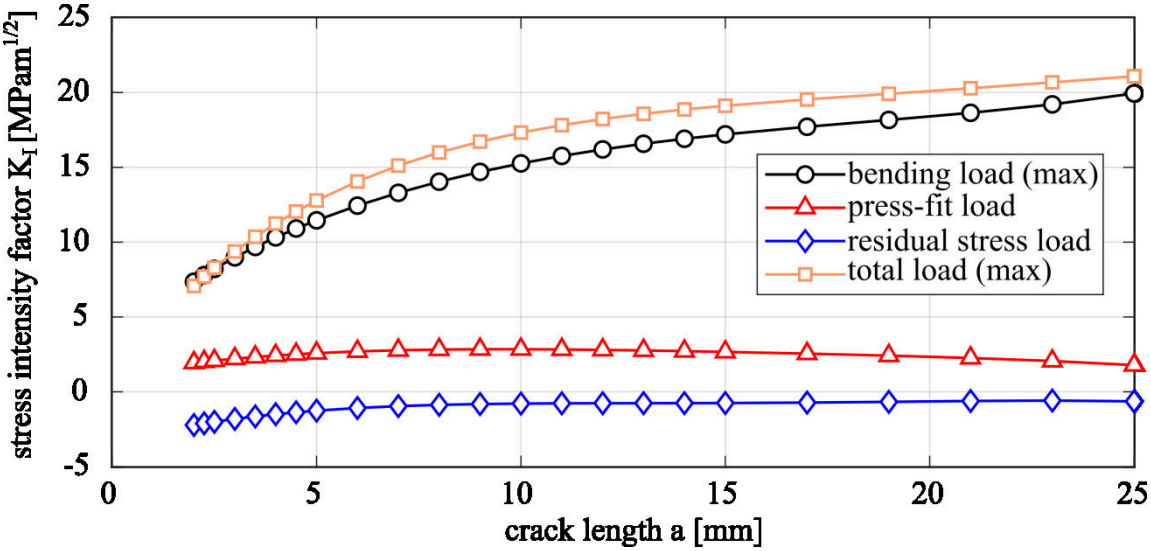


Fig. 17 – K_I values vs crack length a for the standard hardened axle

The results of all SIF components and the total SIF as a dependence on the crack length a are presented in Figs. 17 and 18 for the standard hardened axle and the induction-hardened axle, respectively. The data are shown for the maximum dynamic coefficient k = 2.9 from the bending-load spectrum.

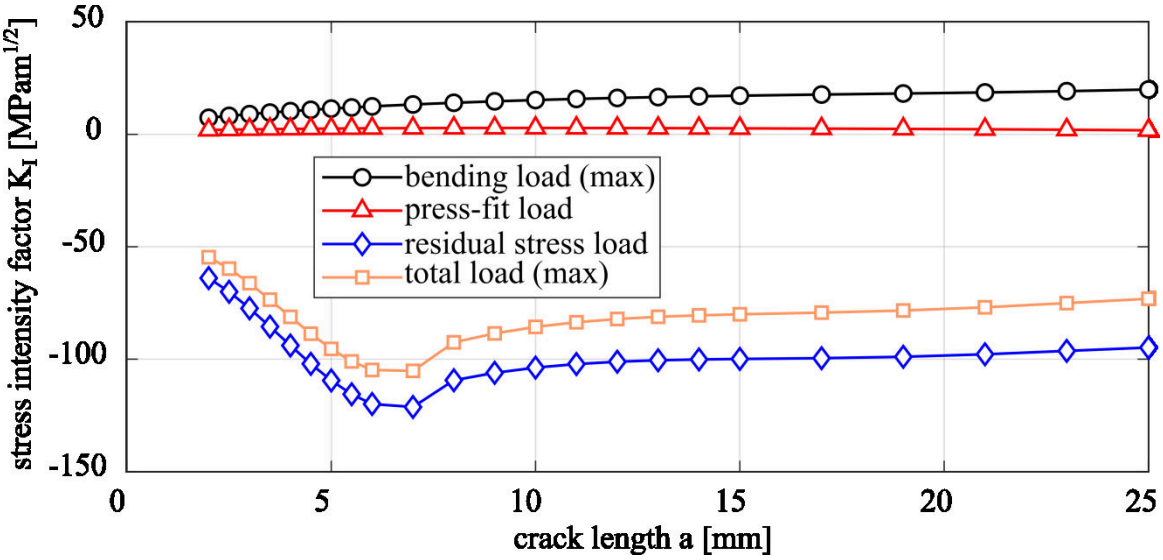


Fig. 18 – K_I values vs crack length a for the induction-hardened axle

3.5 Crack propagation modelling

Due to variable bending load and non-zero mean load the load (stress) ratio was also variable. According to the expressions (3) to (5) the load ratio R is expressed as:

$$R(a,t) = \frac{K_{min}(a,t)}{K_{max}(a,t)} = \frac{K_{PF}(a) + K_{RS}(a) - K_{B,d}(a,t)}{K_{PF}(a) + K_{RS}(a) + K_{B,d}(a,t)} \tag{6}$$

However, it was shown in [36] that fatigue crack propagation for various load ratios in the EA4T steel can be sufficiently described using the $K_{\max}$ parameter, which has almost no dependence on the load ratio R for R less than approximately 0.2. Fig. 19a shows the da/dN-ΔK (fatigue crack propagation) curves experimentally determined for 4 various load ratios R ranging from –2 to 0.1. These data were measured using the center-crack tension (CCT) specimens with the width $2W$ = 60 mm and the thickness t = 5 mm. It was assumed that residual stress in the material was relaxed after fabrication of the CCT specimens and the load ratio was given just by the applied loading. Further details about the experimental determination da/dN-ΔK data can be found in [36] or [14].

The NASGRO equation for description of crack propagation [37] can be used in its original form with ΔK_{eff} as the parameter controlling crack propagation. However, the use of $K_{\max}$ is more suitable for applications with low load ratios, since the threshold value $K_{max,th}$ is nearly constant in range of R from –2 to 0.1, see Fig.19b. It means, that crack closure values are similar in this range of R, including part of oxide-induced crack closure [14,38].

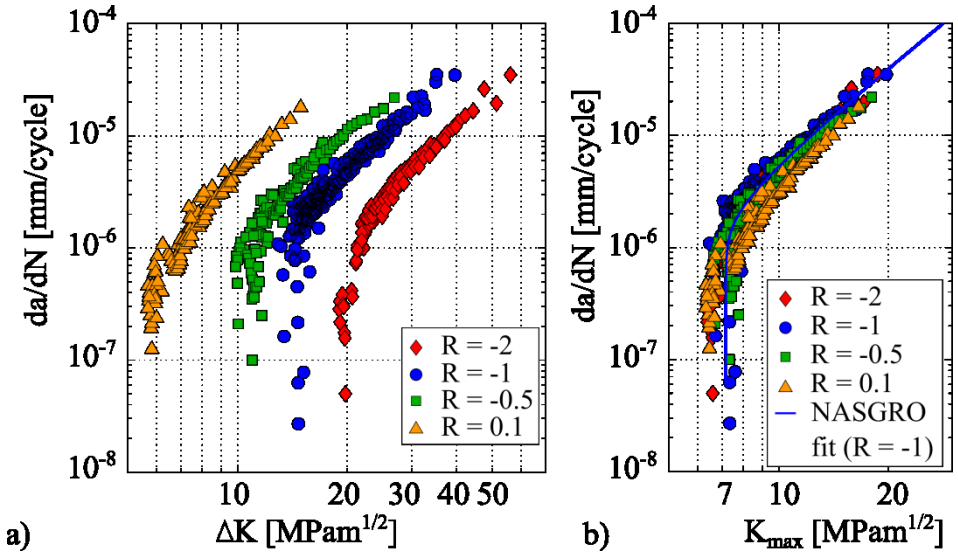


Fig. 19 – Comparison of the fatigue crack growth curves for the standard-hardened EA4T steel a) in *da/dN-ΔK* expression, b) in *da/dN-*K_{max} expression

Using the K_{max} expression (d*a*/d*N*-K_{max}), see Fig. 19b, the fatigue crack propagation curves at different load ratios became overlapped. This represents a huge benefit in the case of the EA4T steel, since only one simple equation with a constant threshold value $K_{max,th}$ can be used for description of crack propagation for the load ratios *R* ranging from –2 up to 0.1. This equation was used in the form of a simplified NASGRO equation:

$$\frac{da}{dN} \cong \frac{\Delta a}{\Delta N} = C(K_{max})^n \left(1 - \frac{K_{max,th}}{K_{max}}\right)^p, \tag{7}$$

where *C*, *n* and *p* are material constants, K_{max} is the maximum SIF (see Eq. (1)), and $K_{max,th}$ is the threshold value of maximum SIF (constant for considered load ratio range).

Fig. 19 shows data measured for specimens fabricated from the surface of the standard heat-treated axle. The induction-hardened specimens were slightly smaller (CCT specimens with the width $2W = 30$ mm and the thickness $t = 4$ mm) compared to the specimens used for the standard heat treated EA4T steel ($2W = 60$ mm, $t = 5$ mm). These specimens were manufactured from surface area of railway axle, see Fig. 20a. Fig. 20b shows comparison of the d*a*/d*N*-K_{max} curves for the standard heat-treated and the induction hardened EA4T steel for stress ratio R = -1. In the case of induction hardened axle the smaller thickness was selected in order to include only the surface layer of the axle affected by induction hardening. Fig. 20b demonstrates that induction hardening reduces the threshold SIF value (in K_{max} expression) from 7.0 MPam$^{1/2}$to 4.6 MPam$^{1/2}$. However, it will be shown later on in this paper that the beneficial effect of residual stresses produced by the induction hardening is much more significant than reduction in the threshold value.

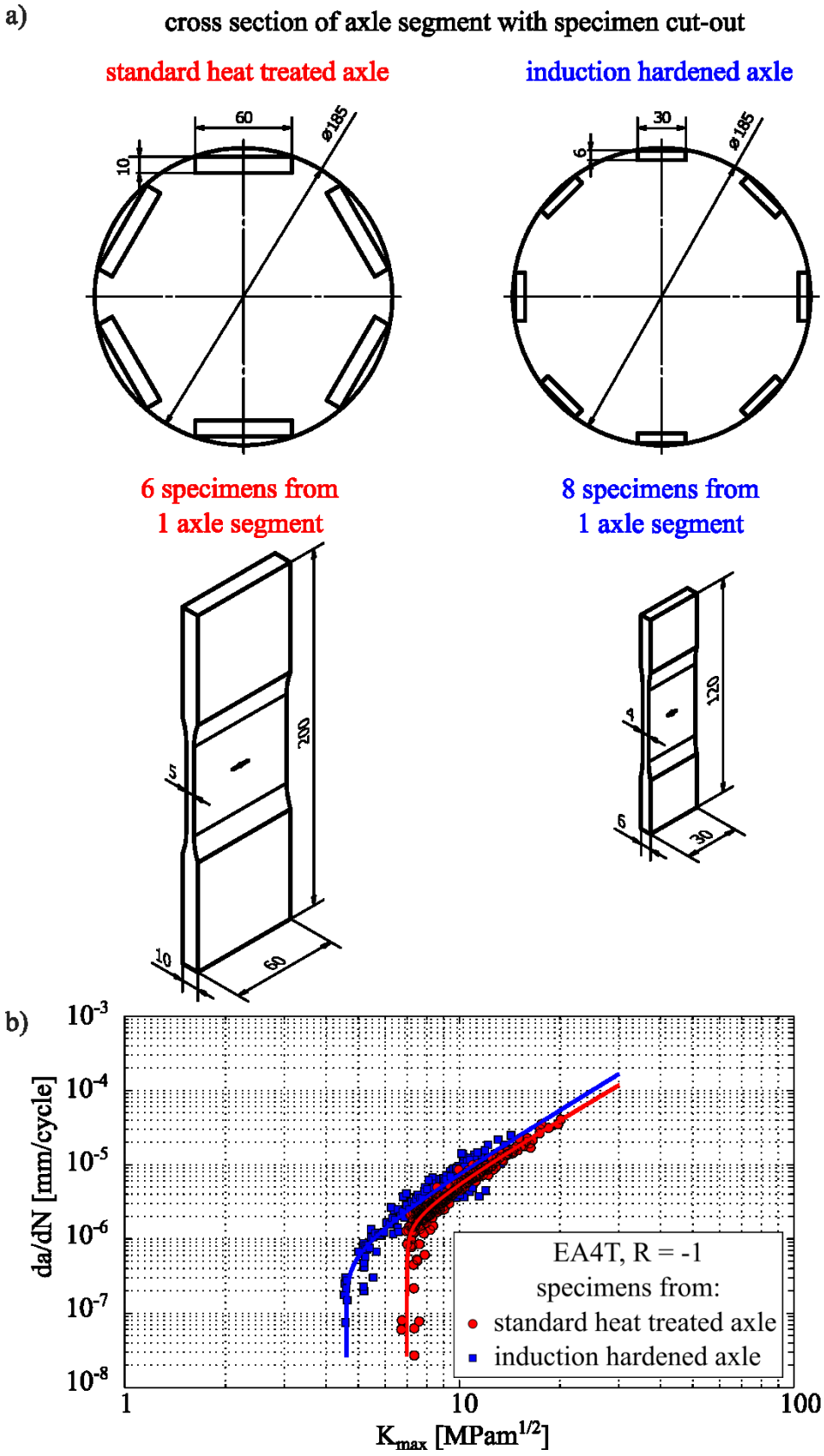


Fig. 20 – a) specimen cut-out and geometry of used specimens b) comparison of the *da/dN-K*$_{max}$ curves of EA4T steel for two types of heat treatment (semi-products for manufacturing of the test specimens were cut from the axle surface area)

Conservative RFLs of the railway axle was calculated as crack propagation period from the initial crack length a_0 up to the length of 25 mm (less than the critical crack length). Propagation of cracks longer than 25 mm is very fast and can be neglected in the whole RFL. The crack length increment Δa was calculated step by step using Eq. (8) for loads $K_{max} > K_{max,th}$ until the crack length a reached the final length:

$$\Delta a = C(K_{max})^n\left(1 - \frac{K_{max,th}}{K_{max}}\right)^p \Delta N. \tag{8}$$

The used constants were: $C = 1.8\times10^{-11}$, $n = 2.6$, $p = 0.25$, $K_{max,th} = 7.0$ MPam$^{1/2}$ for the standard-hardened (heat treated) axle and $C = 1.8\times10^{-11}$, $n = 2.7$, $p = 0.35$, $K_{max,th} = 4.6$ MPam$^{1/2}$ for the induction-hardened axle. For cycles with the maximal load $K_{max} < K_{max,th}$ the crack increments were zero. Calculations run in a loop until the crack length a reached 25 mm:

$$a_i = a_{i-1} + \Delta a \tag{9}$$

where a_i is crack length in the current loop and a_{i-1} is the crack length in the previous one.

The resulting RFL is equal to the sum of the applied loops (1 loop = 1000 km of train service, see Fig. 14). Note that this calculation takes into account no overload cycles that would cause retardation of fatigue crack. This simplification is conservative.

3.6 Calculated results of residual fatigue lives

The results of the estimated values of residual fatigue lives considering residual stress profiles generated by different heat treatments are presented in Table 4. RFLs were determined as a number of kilometres passed by the axle during crack propagation from the initial crack length a_0 (initial crack lengths 2 mm, 3 mm, 5 mm or 10 mm were considered) to the crack length of 25 mm. Results for three different cases of residual stress were obtained: (i) no residual stress, (ii) residual stress produced by standard heat treatment and (iii) residual stresses produced by induction hardening. As expected, the shortest RFLs were estimated for the axle with no residual stress. Axles with residual stress produced by standard heat treatment exhibited much longer RFLs. The influence of residual stresses on RFL is much more pronounced for short initiation crack (2 mm) in comparison with longer initiation cracks (5 mm or 10 mm). This effect is demonstrated in Table 4. The residual stress led to the increase of RFL from 85 000 km to 32 451 000 km for the initial crack length of 2 mm, while the increase of RFL due to residual stress for the initial crack length of 10 mm was from 10 000 km to 13 000 km (only 30%). The reason for this effect is that the compressive residual stresses are induced in the subsurface layers only several millimetres thick (see Table 3) and does not affect importantly propagation of longer cracks.

As was shown in Fig. 20b, the induction hardening reduces the threshold value of SIF $K_{max,th}$ from 7.0 MPam$^{1/2}$ to 4.6 MPam$^{1/2}$. On the other hand, induction hardening results in extremely high compressive stress values in the outer surface layers of a railway axle, which leads to significant reduction of the resultant crack opening load. As a consequence, the crack loading is reduced below the threshold SIF value for all considered initial cracks lengths (from 2 to 10 mm). This is also evident from Fig.18 where the total load K_{max} is negative in the whole

considered range of crack lengths (1 – 25 mm). The considered surface crack does not propagate at all under the considered conditions in the case of induction-hardened axles, which results in theoretically infinite RFLs, see Table 4. It can be concluded that appropriate parameters of induction hardening of the axle leads to development of residual stresses, which prevents the surface fatigue cracks from propagation.

Table 4 – Estimated values of residual fatigue life (in *km)* for different initial crack lengths and method of heat treatment (source of RS) of railway axle

Considered source of residual stresses	initial crack length a_0			
	2 mm	3 mm	5 mm	10 mm
no RS	85 000	35 000	16 000	10 000
RS due to standard hardening	32 451 000	154 000	33 000	13 000
RS due to induction hardening	inf.	inf.	inf.	inf.

4 Experimental validation of calculated residual fatigue lives

The procedures described above, i. e. procedures taking into account influence of the press-fit and residual stresses were experimentally validated using real-scale specimens. For this purpose specimens corresponding to circa one half of the real axle were prepared (see Fig. 21). Artificial semi-elliptical notch was prepared by spark erosion method at the T-notch position of the axle (the same position as in the theoretical considerations). The dimensions of the prepared notch were $2b_n$ 3.75 mm (notch width) and a_n = 1.5 mm the (notch depth), see Fig. 21. The axle specimens were clamped on the wheel and the load was applied by means of an unbalanced mass vibration generator. The spark-eroded notch enabled formation of the crack at the required position. Fatigue precrack was initiated in the notch before beginning of experimental measurement. The initiation of fatigue crack was performed by application of the highest load amplitude from the load spectrum, see Fig. 14.

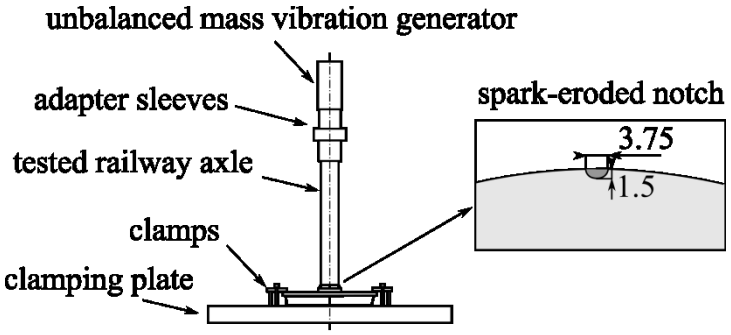


Fig. 21 – Scheme of experimental test

4.1 Testing of standard heat-treated railway axles

Three specimens treated by standard heat treatment were tested. The fatigue pre-cracking was performed applying the maximum load amplitude from the load spectrum (dynamic coefficient k = 2.9). The process of pre-cracking was stopped when the total crack length (notch + fatigue crack) reached depth 2.0 ÷ 2.5 mm. After pre-cracking, the specimens

were subjected to the variable amplitude loading in decreasing sequence of load amplitudes, i. e. the load amplitudes were varied gradually from the highest value to the lowest one. The load spectrum (shown in Fig. 14) was applied 1200 times, which corresponded to 1 200 000 km of train operation. At the end of the tests the specimens were cut to observe the fracture surfaces and evaluate the crack fronts. Fig. 22 shows 3 important stages of the crack/notch. The subscript *n* refers to the notch, the subscript *0* refers to the initial crack dimensions and the subscript *f* represents the final size of the fatigue crack.

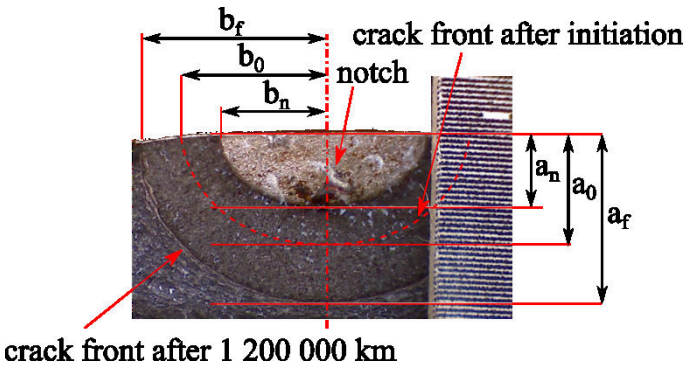


Fig. 22 – Fracture surface after the experiment. Important dimensions and crack front shape are marked

The dimension b was measured optically on the axle surface during the test. The initial crack length a_0 was derived from b_0. It was considered that the ratio between the notch semi-axes and the initial crack semi-axes were equal: $\frac{a_n}{b_n} = \frac{1.5}{3.75/2} = \frac{a_0}{b_0}$, where a_n and b_n are the notch dimensions. After crack initiation, the crack width b_0 was measured and a_0 was obtained as: $a_0 = \frac{1.5}{3.75/2} b_0$. The final crack dimensions a_f and b_f were optically measured at the fracture faces after the test, see Fig. 22. The dimensions measured during three tests performed are summarized in the Table 5.

The resulting lifetime were compared with the results of numerical simulations (considering residual stresses after standard heat treatment and considering axle without residual stress) and summarized in Table 5. Note that the experiments were performed with specimens after induction hardening as well, which is presented in the following Section.

Table 5 – Experimental and calculated results for three standard heat-treated axles

axle	initial crack length a_0	final crack length a_f	tested distance	calculated distance (with RS)	calculated distance (without RS)
axle 1	2.28 mm	3.05 mm	1 200 000 km	185 000 km	26 000 km
axle 2	2.08 mm	2.70 mm	1 200 000 km	497 000 km	34 000 km
axle 3	2.20 mm	3.00 mm	1 200 000 km	217 000 km	31 000 km

Table 5 reveals that the calculated results are conservative in comparison with the performed experiments. This is expected and also desired, since conservative envelope of the measured residual stresses (see black line in Fig. 4) was used for the RFL estimation and the results should be on the safe side. Omission of residual stress in the procedure of RFL estimation

leads to mileages shorter by two orders of magnitude compared to the experiment, see Table 5. The model considering residual stress provides ca $2-6$ times shorter mileages than experimental tests, see Table 5. The presented numerical model taking into account the residual stress field provides relatively accurate conservative estimations of RFLs (depending on the input residual stress data). The described procedure allows the use of other measured residual stress profiles for estimations of RFL. Note that propagation of relatively short cracks was considered in the experiments. Propagation of such cracks is sensitive to the residual stress distribution, the load spectrum and the material threshold value, see the differences in RFLs for initial crack lengths $a_0 = 2$ mm (RFL is 32.5 million km) and $a_0 = 3$ mm (RFL is only 154 000 km). For longer cracks, the difference in RFLs would not be that different. Crack retardation effects (e. g., overloads) were neglected in the RFL estimations. These effects can increase RFL of railway axles in operation. Nevertheless, the load spectrum during the experiments was applied in gradual decreasing sequence of load amplitudes (it is not possible to apply rapid changes of the load amplitude using the resonant testing machine) which led to minimization of the retardation effects. Therefore experimentally determined and calculated RFLs should be both comparable and conservative in the comparison with real operation.

4.2 Testing of induction-hardened railway axles

The next experiments were focused on the induction-hardened axles and followed the same procedure, setup and notch parameters as described for the standard heat-treated axles. Based on the gathered numerical results (see Table 4), it was expected that a higher load than the maximum load from the service load spectrum would be needed for the crack initiation and growth. Therefore, cyclic loading was applied with the value corresponding to the nominal stress amplitude of 200 MPa (the dynamic coefficient $k = 5.2$). This value is much higher than the maximum load in the load spectrum (Fig. 14). Nevertheless, no crack propagation occurred after application of 5×10^6 cycles. Therefore, the load amplitude was further increased to 280 MPa for 10^7 cycles and then again to 300 MPa for 10^7 cycles. Even two-fold increase in the load amplitude did not lead to crack propagation from the initial notch. Finally, fatigue crack propagation was achieved after 1.1×10^6 cycles at the level of nominal stress of 340 MPa. Such load level corresponds to the dynamic coefficient $k = 8.8$ (i.e. 8.8× higher load than in the static load case). The test was terminated due to excessive load of the experimental stand. The experiment confirmed that application of the standard load spectrum leads to no fatigue crack initiation and propagation in the case of induction-hardened axles with considered surface cracks.

5 Conclusions

The influence of residual stress on residual fatigue life of railway axles was studied and discussed in this paper. Two types of axle heat treatment were considered in the theoretical and experimental studies: standard heat treatment (standard hardening) and induction hardening. A distribution of residual stresses was experimentally determined using the drilling method. An extensive FE modelling was used for backward determination of original residual stress distribution before turning process. In the following step the stress intensity factors including the residual stress effects were numerically determined for axles treated by both considered

types of heat treatment. These input data enabled correct simulation of crack propagation and more precise residual fatigue life estimation. On the basis of the experimental and theoretical results the following conclusions can be drawn:

- Compressive residual stress generated under the axle surface significantly reduced driving force of surface cracks and defects. Therefore, the residual fatigue life of these axles was substantially longer than in the case of axles with no residual stress.
- The described effect of residual stress on the residual fatigue life was more pronounced for axles with shorter initial cracks.
- The residual fatigue life estimated by authors' original numerical approach considering residual stresses was close to the experimental results obtained for real axle pieces. The estimated RFL was 2 – 6 times shorter than the experimental one in the case of standard heat-treated axles. The apparent underestimation of RFL was given by conservative consideration of residual stress profiles.
- It was shown that induction hardening generates extremely high compressive residual stress (with the absolute peak value of approx. 850 MPa) with a large extent of the negative axial stress component into the depth below the axle surface of 15 – 20 mm. Such residual stress prevented all considered surface cracks from propagating, as was predicted by the presented procedure of RFL estimation and also proved by experiments.
- The presented procedure enables quite accurate estimation of residual fatigue life of railway axles, when knowledge of the residual stress profiles in the axles is good and the measured residual stresses are appropriately post-processed.

Acknowledgement

The work was supported through the grant No. FV40034 “Development of new design of railway axles with high operational reliability” of the Ministry of Industry and Trade of the Czech Republic. The cooperation between Institute of Physics of Materials CAS and Bonatrans Group was realized in the frame of Strategy 21 “Top research in the public interest” of Czech Academy of Sciences. International co-operation was supported by KMM-VIN Research Fellowship (call 9).

References

[1] U. Zerbst, S. Beretta, G. Köhler, A. Lawton, M. Vormwald, H.T.T. Beier, C. Klinger, I. Černý, J. Rudlin, T. Heckel, D. Klingbeil, Safe life and damage tolerance aspects of railway axles – A review, Eng. Fract. Mech. 98 (2013) 214–271. doi:10.1016/j.engfracmech.2012.09.029.

[2] C. Klinger, D. Bettge, Axle fracture of an ICE3 high speed train, Eng. Fail. Anal. 35 (2013) 66–81. doi:10.1016/j.engfailanal.2012.11.008.

[3] Z. Odanovic, M. Ristivojevic, V. Milosevic-Mitic, Investigation into the causes of

fracture in railway freight car axle, Eng. Fail. Anal. 55 (2015) 169–181. doi:10.1016/j.engfailanal.2015.05.011.

[4] Railway Safety Performance in the European Union 2016, 2016. http://www.era.europa.eu/Document-Register/Pages/Railway-Safety-Performance.aspx.

[5] R.A. Smith, Fatigue of railway axles: A classic problem revisited, in: 2000: pp. 173–181. doi:10.1016/S1566-1369(00)80049-7.

[6] U. Zerbst, K. M€ Adler, H. Hintze, K. Mädler, H. Hintze, Fracture mechanics in railway applications—an overview, Eng. Fract. Mech. 72 (2005) 163–194. doi:10.1016/j.engfracmech.2003.11.010.

[7] M. Luke, I. Varfolomeev, K. Lütkepohl, A. Esderts, Fracture mechanics assessment of railway axles: Experimental characterization and computation, Eng. Fail. Anal. 17 (2010) 617–623. doi:10.1016/j.engfailanal.2009.04.008.

[8] Z. Odanovic, Analysis of the railway freight car axle fracture, Procedia Struct. Integr. 4 (2017) 56–63. doi:10.1016/j.prostr.2017.07.009.

[9] D. Regazzi, S. Cantini, S. Cervello, S. Foletti, Optimization of the cold-rolling process to enhance service life of railway axles, Procedia Struct. Integr. 7 (2017) 399–406. doi:10.1016/j.prostr.2017.11.105.

[10] S. Beretta, M. Carboni, D. Regazzi, Load interaction effects in propagation lifetime and inspections of railway axles, Int. J. Fatigue. (2016) 423–433. doi:10.1016/j.ijfatigue.2016.03.009.

[11] M. Traupe, S. Jenne, K. Lütkepohl, I. Varfolomeev, Experimental validation of inspection intervals for railway axles accompanying the engineering process, Int. J. Fatigue. 86 (2016) 44–51. doi:10.1016/j.ijfatigue.2015.09.020.

[12] M. Luke, M. Burdack, S. Moroz, I. Varfolomeev, Experimental and numerical study on crack initiation under fretting fatigue loading, Int. J. Fatigue. 86 (2016) 24–33. doi:10.1016/j.ijfatigue.2015.09.022.

[13] P. Pokorný, P. Hutař, L. Náhlík, Residual fatigue lifetime estimation of railway axles for various loading spectra, Theor. Appl. Fract. Mech. 82 (2016) 25–32. doi:10.1016/j.tafmec.2015.06.007.

[14] P. Pokorný, T. Vojtek, L. Náhlík, P. Hutař, Crack closure in near-threshold fatigue crack propagation in railway axle steel EA4T, Eng. Fract. Mech. 185 (2017) 2–19. doi:10.1016/j.engfracmech.2017.02.013.

[15] T. Oplt, M. Šebík, F. Berto, L. Náhlík, P. Pokorný, P. Hutař, Strategy of plasticity induced crack closure numerical evaluation, Theor. Appl. Fract. Mech. 102 (2019) 59–69. doi:10.1016/j.tafmec.2019.04.004.

[16] S.C. Wu, S.Q. Zhang, Z.W. Xu, G.Z. Kang, L.X. Cai, Cyclic plastic strain based damage tolerance for railway axles in China, Int. J. Fatigue. 93 (2016) 64–70. doi:10.1016/j.ijfatigue.2016.08.006.

[17] M.N. James, D.G. Hattingh, D. Asquith, M. Newby, P. Doubell, Residual stresses in

condition monitoring and repair of thermal power generation components, Theor. Appl. Fract. Mech. 92 (2017) 289–297. doi:10.1016/j.tafmec.2017.03.008.

[18] D. Regazzi, S. Beretta, M. Carboni, An investigation about the influence of deep rolling on fatigue crack growth in railway axles made of a medium strength steel, Eng. Fract. Mech. 131 (2014) 587–601. doi:10.1016/j.engfracmech.2014.09.016.

[19] S.M. Hassani-Gangaraj, M. Carboni, M. Guagliano, Finite element approach toward an advanced understanding of deep rolling induced residual stresses, and an application to railway axles, Mater. Des. 83 (2015) 689–703. doi:10.1016/j.matdes.2015.06.026.

[20] H.-P.P. Gänser, J. Maierhofer, R. Tichy, I. Zivkovic, R. Pippan, M. Luke, I. Varfolomeev, Damage tolerance of railway axles – The issue of transferability revisited, Int. J. Fatigue. 86 (2016) 52–57. doi:10.1016/j.ijfatigue.2015.07.019.

[21] L. Náhlík, P. Pokorný, M. Ševčík, R. Fajkoš, P. Matušek, P. Hutař, Fatigue lifetime estimation of railway axles, Eng. Fail. Anal. 73 (2017) 139–157. doi:10.1016/j.engfailanal.2016.12.014.

[22] M. Madia, S. Beretta, U. Zerbst, An investigation on the influence of rotary bending and press fitting on stress intensity factors and fatigue crack growth in railway axles, Eng. Fract. Mech. 75 (2008) 1906–1920. doi:10.1016/j.engfracmech.2007.08.015.

[23] S.C. Wu, Y.X. Liu, C.H. Li, G.Z. Kang, S.L. Liang, On the fatigue performance and residual life of intercity railway axles with inside axle boxes, Eng. Fract. Mech. 197 (2018) 176–191. doi:10.1016/j.engfracmech.2018.04.046.

[24] O. Yasniy, Y. Lapusta, Y. Pyndus, A. Sorochak, V. Yasniy, Assessment of lifetime of railway axle, Int. J. Fatigue. 50 (2013) 40–46. doi:10.1016/j.ijfatigue.2012.04.008.

[25] R. Hannemann, M. Sander, Effect of Specimen Geometry and Press-Fit on the Stress Intensity Factor Solution for Scaled Wheelset Axles under Bending, Procedia Struct. Integr. 2 (2016) 2527–2534. doi:10.1016/j.prostr.2016.06.316.

[26] P. Hutař, P. Pokorný, J. Poduška, R. Fajkoš, L. Náhlík, Effect of residual stresses on the fatigue lifetime of railway axle, Procedia Struct. Integr. 4 (2017) 42–47. doi:10.1016/j.prostr.2017.07.005.

[27] X. Lorang, Y. Cheynet, P. Feraud, Y. Nadot, A study on lifetime of a railway axle subjected to grinding, Procedia Eng. 213 (2018) 255–261. doi:10.1016/j.proeng.2018.02.026.

[28] J.W. Zhang, L.T. Lu, K. Shiozawa, X.L. Shen, H.F. Yi, W.H. Zhang, Analysis on fatigue property of microshot peened railway axle steel, Mater. Sci. Eng. A. 528 (2011) 1615–1622. doi:10.1016/j.msea.2010.10.086.

[29] T. Makino, H. Sakai, Fatigue Property of Railway Axles for Shinkansen Vehicles, technical report., 2013.

[30] S. Isomura, K. Yomoda, Manufacturing history of axles for Shinkansen, in: Proc. 11th Int. Wheel. Congr. Natl. Conf. Publ. Aust. Vol. 2, Pp. 51–54., 1995.

[31] S.C. Wu, Z.W. Xu, Y.X. Liu, G.Z. Kang, Z.X. Zhang, On the residual life assessment of high-speed railway axles due to induction hardening, Int. J. Rail Transp. 6 (2018)

218–232. doi:10.1080/23248378.2018.1427008.

[32] H. Gong, Y. Wu, X. Feng, Y. Li, Analysis of quenching stresses in 35CrMo axle, J. Wuhan Univ. Technol. Sci. Ed. 31 (2016) 630–635. doi:10.1007/s11595-016-1421-9.

[33] J. Vázquez, C. Navarro, J. Domínguez, A model to predict fretting fatigue life including residual stresses, Theor. Appl. Fract. Mech. 73 (2014) 144–151. doi:10.1016/j.tafmec.2014.06.012.

[34] Schajer GS, Practical resdiual stress measurement methods, 2013.

[35] T.L. Anderson, Fracture mechanics: fundamentals and applications. 3rd ed. Boca Raton, FL: Taylor & Francis, 2005. ISBN 0849316561., 2005.

[36] P. Pokorný, L. Náhlík, P. Hutař, Influence of variable stress ratio during train operation on residual fatigue lifetime of railway axles, Procedia Struct. Integr. 2 (2016) 3585–3592. doi:10.1016/j.prostr.2016.06.447.

[37] NASGRO, Fracture Mechanics and Fatigue Crack Growth Analysis Software, Reference manual., (2002) 112. www.nasgro.swri.org.

[38] T. Vojtek, P. Pokorný, I. Kuběna, L. Náhlík, R. Fajkoš, P. Hutař, Quantitative dependence of oxide-induced crack closure on air humidity for railway axle steel, Int. J. Fatigue. 123 (2019) 213–224. doi:10.1016/j.ijfatigue.2019.02.019.

DSPACE

https://dspace.org/

Influence of heat treatment-induced residual stress on residual fatigue life of railway axles

Pokorny, Pavel; Dlhý, Pavol; Poduska, Jan; Fajkoš, Rostislav; Vojtek, Tomáš ...

2020-08-03
Elsevier
https://doi.org/10.1016/j.tafmec.2020.102732
Pokorný P, Dlhý P, Poduška J, et al., (2020) Influence of heat treatment-induced residual stress on residual fatigue life of railway axles. Theoretical and Applied Fracture Mechanics, Volume 109, October 2020, Article number 102732

Downloaded from a DSpace repository. https://dspace.org/